https://doi.org/10.26599/JAC.2024.9220911

Research Article

Realizing the excellent oxidation resistance of an environmental barrier coating through aluminum surface modification

Lin Dong[a], Wen-Qi Yang[b], Lin Chen[a]*, Guan-Jun Yang[a], Chang-Jiu Li[a]

[a] State Key Laboratory for Mechanical Behavior of Materials, School of Materials Science and Engineering, Xi'an Jiaotong University, Xi'an 710049, China

[b] Xi'an Aerospace Engine Company Limited in CASC, Xi'an 710065, China

*Corresponding author.

Email address: L. Chen, chenlinxjtu@mail.xjtu.edu.cn

Received: March 08, 2024; Revised: April 23, 2024; Accepted: May 09, 2024

Abstract

The lifetime of Si-based environmental barrier coatings (EBCs) is constrained by thermally grown SiO_2 (SiO_2-TGO), which can cause premature cracking and spalling. To address this issue, a new approach for surface modification using aluminum is proposed. The oxidation performance was examined in a 50 vol% H_2O - 50 vol% O_2 environment at 1350 ℃ for up to 300 h. The results indicate that a dense ytterbium aluminum garnet (YbAG) layer was formed after modification, decreasing the porosity by 80%. Due to the elimination of fast diffusion channels and the low oxygen permeability of YbAG, aluminum modification significantly reduced the growth rate of SiO_2-TGO by nearly two orders of magnitude. Consequently, its thickness decreased by more than 70% after 300 h

of exposure. A diffusion-controlled oxidation mechanism indicates that the modified dense surface is equivalent to an initial SiO_2 layer with a specific thickness, causing a shift in the oxidation time and increasing the oxidation resistance. This research provides valuable insights for designing Si-based EBC with improved lifetimes.

Keywords: Environmental barrier coating (EBC); oxidation; modification; diffusion; cracking.

1. Introduction

SiC-Ceramic Matrix Composites (SiC-CMCs) are crucial materials for combustion components in gas turbine engines. These materials have melting points exceeding 2700 K and are extremely lightweight, providing excellent heat resistance and enhancing fuel efficiency[1-3]. However, SiC-CMC is susceptible to degradation in combustion environments containing high-temperature water vapor and oxygen [4, 5]. Therefore, the surface should be covered with dense environmental barrier coatings (EBCs) to provide superior shielding against corrosive atmospheres for the application of hot section components [1, 2, 6].

In recent decades, multilayered EBC systems have been widely studied for their ability to achieve excellent combinations of properties, including high volatilization and oxidation resistance, good thermomechanical compatibility, and strong bonding strength. The most promising system consists of a protective top layer of ytterbium silicate, which includes ytterbium monosilicate (Yb_2SiO_5, YbMS) and ytterbium disilicate ($Yb_2Si_2O_7$, YbDS)[7, 8]; an oxygen shielding intermediate layer, such as mullite (if required)[9-11]; and a bond layer, such as silicon, to enhance the adhesion strength and oxidation resistance of the substrate[12-14]. When operating in a high-temperature oxidative environment, oxidants penetrate the outer layers to reach the silicon surface, leading to the formation of a thermally grown SiO_2 oxide layer (SiO_2-TGO). Upon cooling, the β-α phase transforms of SiO_2 at 220 ℃, resulting in an ~4.9% volume shrinkage [15, 16]. This causes cracking of SiO_2-TGO, which is one of the main failure modes of EBC. Thus, methods to enhance

the oxidation resistance of EBC systems in hot water vapor and oxygen environments have received considerable attention.

Oxidant transport controls the SiO_2-TGO growth rate and thus determines the EBC life. There are three main transfer pathways for oxidants in EBC. One pathway is diffusion across the lattice through defect reactions between oxygen and ytterbium ions with vacancies. The calculated oxygen permeability constant of ytterbium disilicate is an order of magnitude greater than that of SiO_2-TGO [17, 18]. Another pathway is diffusion across grain boundaries, which has been directly measured and proven to be a preferential diffusion channel over the lattice in dense coating systems [19-21]. These studies were carried out using wafers, which are dense enough without crack defects. In fact, in the widely accepted air plasma sprayed (APS) EBC system, due to insufficient bonding of adjacent splats and preparation quenching stress, pores and cracks inevitably form and connect on a three-dimensional scale [18, 22, 23]. This is the third transfer path for oxidants and is the fastest and the most preferred diffusion path; as a result, the oxidants flow directly in molecular patterns without shielding or going through defective reactions [17, 23, 24].

To reduce the flux of oxidants reaching the silicon surface, extensive efforts have been made by many groups. The most effective way to prevent oxidant diffusion is to produce densely structured EBC by optimizing the deposition parameters [12, 25-28]. Nevertheless, it is difficult to completely eliminate interconnected microcracks in the as-sprayed microstructure [29, 30]. It has also been verified that the addition of modifiers (such as Al_2O_3 and Al_2O_3-containing compounds) to the top layer can effectively hinder oxygen ion permeation and thus reduce the SiO_2-TGO growth rate by 87% [15, 31, 32]. In addition, several efforts have been made to stabilize the β-cristobalite phase transformation to an integrated SiO_2-TGO structure by incorporating cations such as Al^{3+}, Hf^{2+}, and Sr^{2+} [33, 34]. These methods reduce the oxygen diffusion rate and inhibit the phase transformation of SiO_2-TGO to a certain extent but have little effect on eliminating the rapid diffusion channels present in the outer layers, which also significantly affects the oxidation resistance.

This work aimed to improve the oxidation resistance of YbMS/mullite/Si coatings deposited by APS through aluminum modification and further improve their service life in an oxidizing environment. On the one hand, a dense top layer was obtained through aluminum infiltration to eliminate fast diffusion channels, and on the other hand, a continuous thin barrier film with a low diffusion coefficient for oxidants was simultaneously formed on the surface. The oxidation kinetics of the modified coating in a 50 vol% H_2O - 50 vol% O_2 environment at 1350 ℃ were further investigated. Furthermore, the dominant mechanism of oxidation resistance and subsequent improvement in life were elucidated. The results showed that the Yb_2SiO_5/mullite/Si EBC was dense after aluminum modification, which contributed to a reduced oxidation rate and further improved service life in an oxidative environment. This is mainly due to the enhanced pore transport resistance of the top layer. This work demonstrated a post modification approach for designing an EBC system with excellent oxidation resistance.

2. Experimental procedures

2.1 Coating preparation

In this work, Yb_2SiO_5/mullite/Si trilayer coatings were first deposited on a sandblasted rough SiC substrate by a commercial APS system (GP-80). Crushed silicon and mullite particles with a size distribution of 10 to 40 μm were used. The particle size of the agglomerated YbMS powders ranged from 15 to 60 μm. The roughness (*R*a) of the SiC substrate was ~5 μm. The thickness of each layer was approximately 50~80 μm. The deposition parameters are listed in Table 1.

Table 1 APS deposition parameters of the Yb_2SiO_5/mullite/Si trilayer coatings

Materials	Current (A)	Plasma gas (slpm)	Feed rate (g/min)	Stand-off distance (mm)	Preheating (℃)
Si	600	Ar/H_2=40:3	14	130	~150
Mullite	630	Ar/H_2=40:8	15	130	~200
Yb_2SiO_5	630	Ar/H_2=43:8	23	130	~150

Subsequently, a metallic aluminum film of approximately 3 μm was deposited on the surface of the EBC by the vacuum magnetron sputtering technique (J-1250, Jingzhou

Industrial Coating, China). After that, the samples were heated in a vacuum furnace at 750 ℃ for 20 min at a heating rate of 4 ℃·min^{-1}. Then, high-purity argon gas (Ar purity≥99.999%, O_2<0.001 ppm) was gradually backfilled into the furnace until the pressure reached 1.0×10^5 Pa and held for 60 min to ensure that molten aluminum was pressed into the connected pores and microcracks [23]. Finally, the infiltrated samples were heat-treated at 1100 ℃ in the same controlled atmosphere (Ar purity≥99.999%, O_2<0.001 ppm) for 2 h and cooled to room temperature at a rate of 4 ℃·min^{-1}. The aluminum-modified coatings were thus prepared. For comparison, the as-sprayed trilayer coatings were simultaneously heat-treated at 1100 ℃ for 2 h in a controlled atmosphere (Ar purity≥99.999%, O_2<0.001 ppm).

2.2 Oxidation test and microstructural characterization

Oxidation tests of the as-sprayed coatings and aluminum-modified coatings were carried out isothermally in an Al_2O_3 tube furnace at 1350 ℃ and 1.0×10^5 Pa for up to 300 h. A wet oxidative atmosphere of 50 vol.% H_2O – 50 vol.% O_2 was injected into the furnace at a flow rate of 2 L·min^{-1}.

The surface and cross-sectional morphologies of the specimens were characterized by scanning electron microscopy (SEM, MIRA 3 LMH, Tescan) in both secondary electron (SE) mode and back-scattered electron (BSE) mode. The porosity of the coatings was measured through image analysis of 10 images of the same viewable range. The coating surface phase composition was characterized via X-ray diffraction (XRD, D8 ADVANCE, Bruker, DEU) in the 2θ configuration from 10° to 90°. Elemental distributions were analyzed via energy dispersive spectroscopy (EDS, AZTEC, Oxford Instruments) coupled with SEM. To determine the microscopic structure and crystal composition, the modified coatings were also observed using transmission electron microscopy (TEM, Titan Themis 200, FEI). The TEM samples were prepared by focused ion beam (FIB, 450S, FEI) milling. Digital Micrograph software was used to analyze the spectra.

3. Results

3.1 Structural evolution after aluminum modification

Figure 1 shows the microstructure of the as-sprayed coating. The surface was rough

with numerous splashes and unmelted particles, as shown in Fig. 1a. The measured surface roughness *Ra* is approximately 6.1±0.8 μm. A large number of micron-scale cracks and pores are clearly exposed on the surface. The polished cross-sectional image displayed a distinct lamellar structure (Fig. 1b), with considerable interlaminar and vertical cracks forming interconnected networks. The formation of interlaminar cracks is mainly caused by insufficient bonding between adjacent splats due to the low deposition temperature, as well as the presence of unmelted and semimelted particles in the flame. Vertical cracks are generated due to the inherent quenching stress and thermal mismatch stress between the YbMS layer and the SiC substrate during deposition. Channel cracks even formed throughout the entire thickness. It can be inferred that these cracks and pores exhibit stronger continuity at the three-dimensional scale. The measured porosity of the as-sprayed top layer was approximately 6.2% ± 1.2%. These results indicate that the as-sprayed coating has a porous structure, significantly reducing its oxidation resistance.

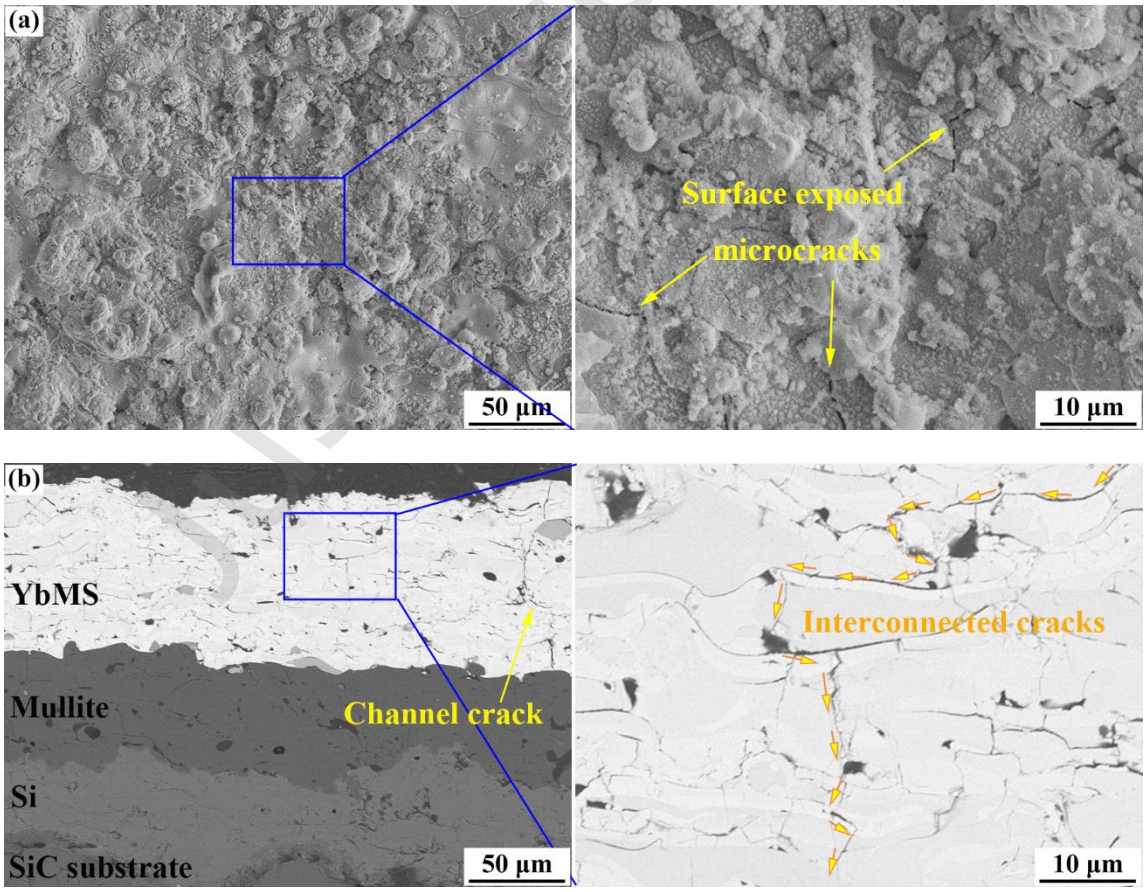

Fig. 1 Surface (a) and cross-sectional (b) microstructures of the as-sprayed coating.

After aluminum modification, the coating exhibited a much denser structure. As seen

from the surface morphology in Fig. 2a, the original cracks were sealed, with no obvious exposed entrances. The cross-sectional morphology in Fig. 2b confirmed that the cracks were completely filled. In addition, a reaction layer of approximately 5~10 μm with different contents was formed at the surface, resulting in a more uniform surface than that of the as-sprayed coating. The measured roughness was 5.2 ± 0.6 μm, which is slightly lower than that before modification. The porosity of the modified coating decreased to 1.1% ± 0.4%, which was more than 80% lower than that of the as-sprayed coating. This difference was mainly attributed to the filling of interconnected pores by aluminum after modification. The remaining porosity was mainly due to internal isolated pores, which are difficult to fill. These isolated pores within the coating facilitate the release of stored strain energy and reduce stress-induced cracking or delamination. These results indicate that aluminum modification can effectively eliminate channel cracks in the as-sprayed coating, significantly increasing its oxidation resistance.

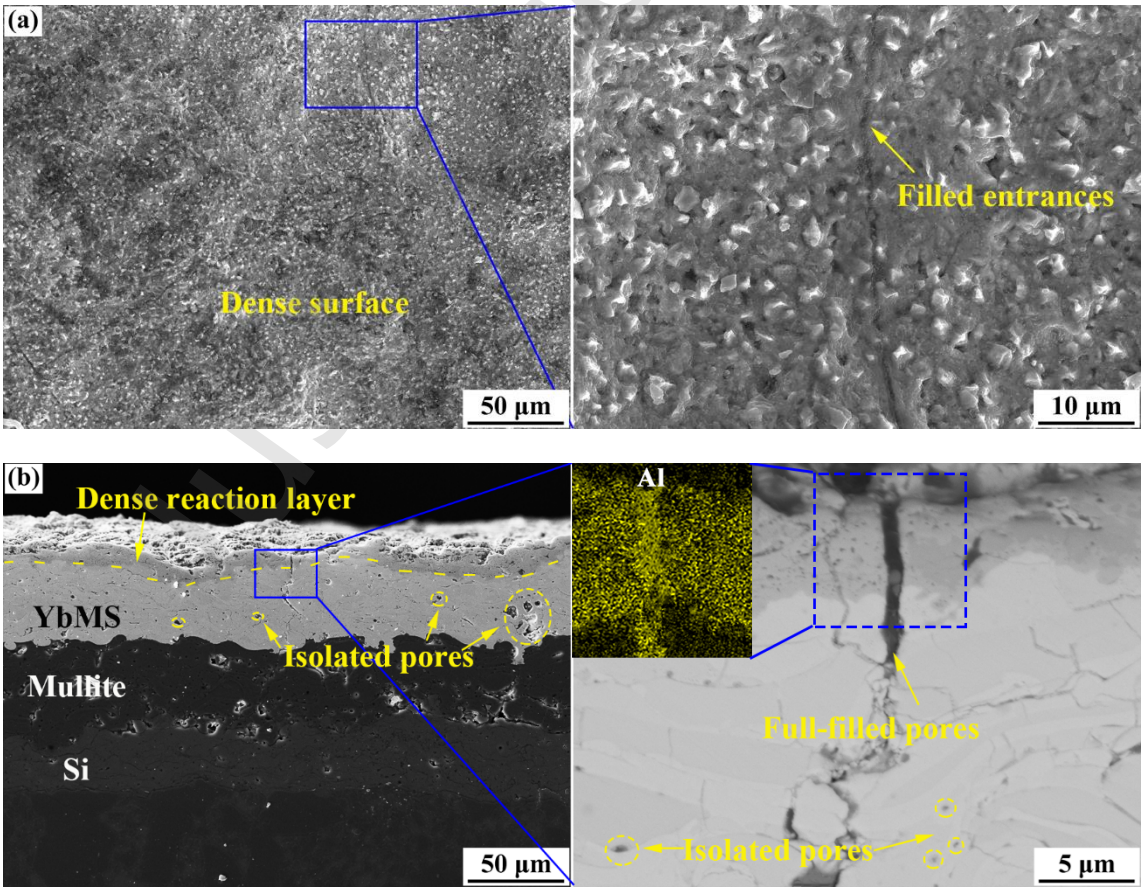

Fig. 2 Surface (a) and cross-sectional (b) microstructures of the modified coating.

Fig. 3 shows the phase composition of the as-sprayed and aluminum-modified

coatings. There were two main phases in the as-sprayed sample: ytterbium monosilicate (YbMS, major) and ytterbium oxide (Yb_2O_3, minor). The main peaks of the YbMS and Yb_2O_3 phases are at (1-3 1) and (2 2 2), with corresponding 2θ values of 29.6° and 23.0°, respectively. The Yb_2O_3 phase content was estimated to be 35.1 wt.%, which was attributed to the partial decomposition of YbMS during deposition. After aluminum modification, ytterbium aluminum garnet ($Yb_3Al_5O_{12}$, YbAG) was detected. The main peak of the YbAG phase is at (4 2 0), with a corresponding 2θ value of 33.6°. The YbAG phase content was estimated to be 64.7 wt.%, which is the continuous main phase of the surface reaction layer. The Yb_2O_3 phase content decreased to 6.4 wt.%, and it was inferred that Yb_2O_3 is one of the reactants participating in the surface in situ reaction.

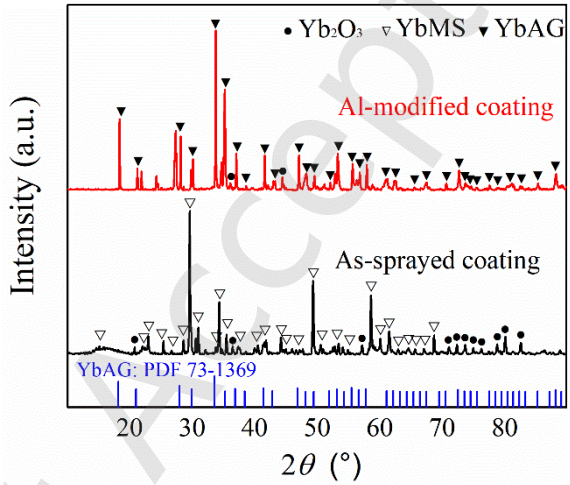

Fig. 3 XRD patterns of the as-sprayed and modified coatings at room temperature.

The composition of the surface reaction layer was further examined, and the results are presented in Fig. 4. Fig. 4a shows a cross-sectional image in BSE mode. These notable differences, in contrast, highlighted the emergence of new phases following the modification. The EDS results in Fig. 4b show that the reaction layer mainly consisted of continuous YbAG phases (points P1 and P2) and dispersed Al-Si-O compounds (point P3). The original YbMS phase became oxygen-rich due to the outward diffusion of Yb and Si (points P4 and P5). Furthermore, the elemental composition of the surface YbAG phase differed slightly between the inner and outer positions, with a lower oxygen content on the outer surface. This phenomenon indicates that the oxygen in the reaction layer mainly originates from ytterbium silicate rather than from the external atmosphere.

TEM analysis was conducted to further confirm the phase composition of the reaction layer. The cross-sectional bright field (BF) image in Fig. 4c exhibited a completely opposite contrast compared with the BSE images. The brightest areas in Fig. 4c represent pores. It is clear that nanoscale and even microscale pores were distributed throughout the reaction layer. Based on the elemental distributions in Fig. 4d, the light gray phase in Fig. 4c and the dark gray phase in Fig. 4a were confirmed to be Al-Si-O compounds. The constituent elements of the surface continuous phases were Yb, Al and O, which was consistent with the point scan result in Fig. 4a. The measured fringe distance of the continuous phase in the high-resolution TEM image (HRTEM) and the corresponding SAD pattern were analyzed to identify the YbAG lattice, as shown in Fig. 4e, which was consistent with the EDS results. These results confirm that a dense YbAG layer was formed after aluminum modification, effectively eliminating the channel cracks in the as-sprayed coating.

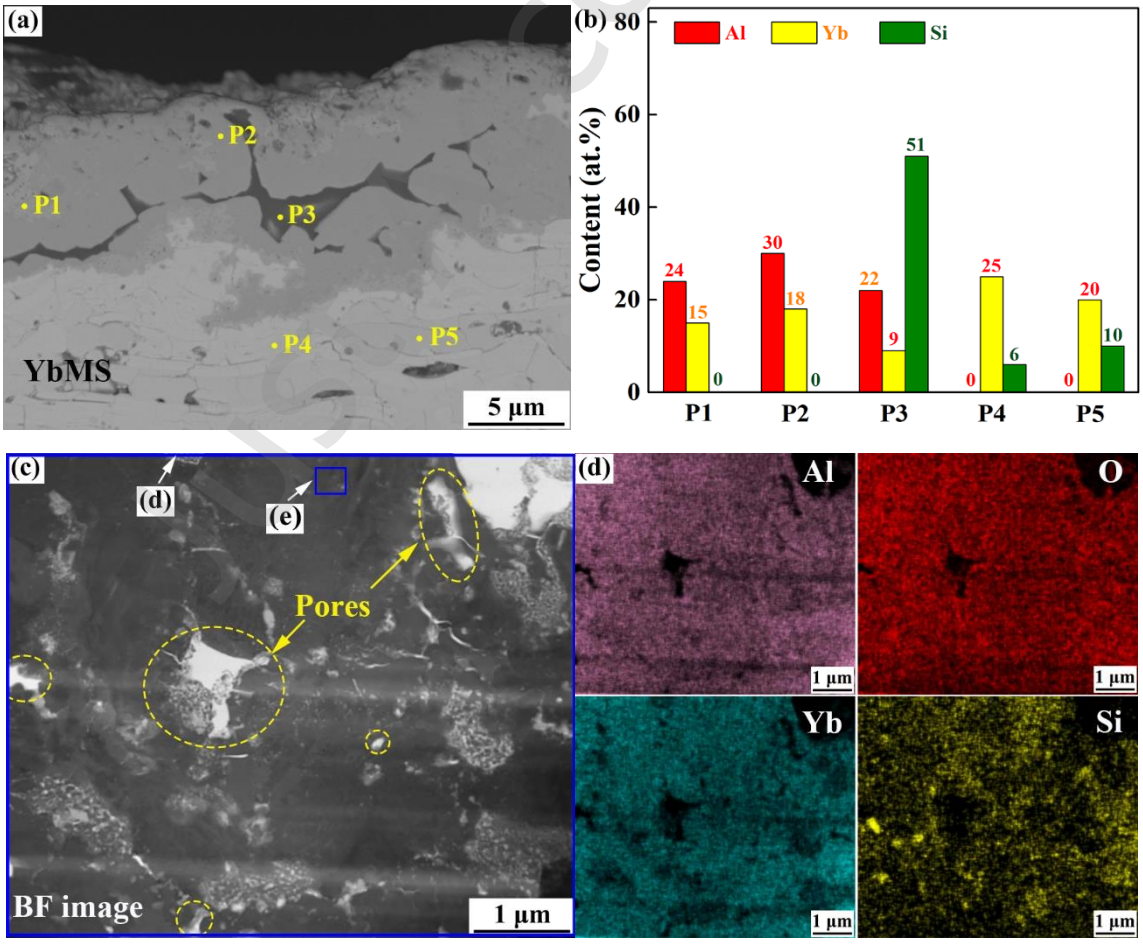

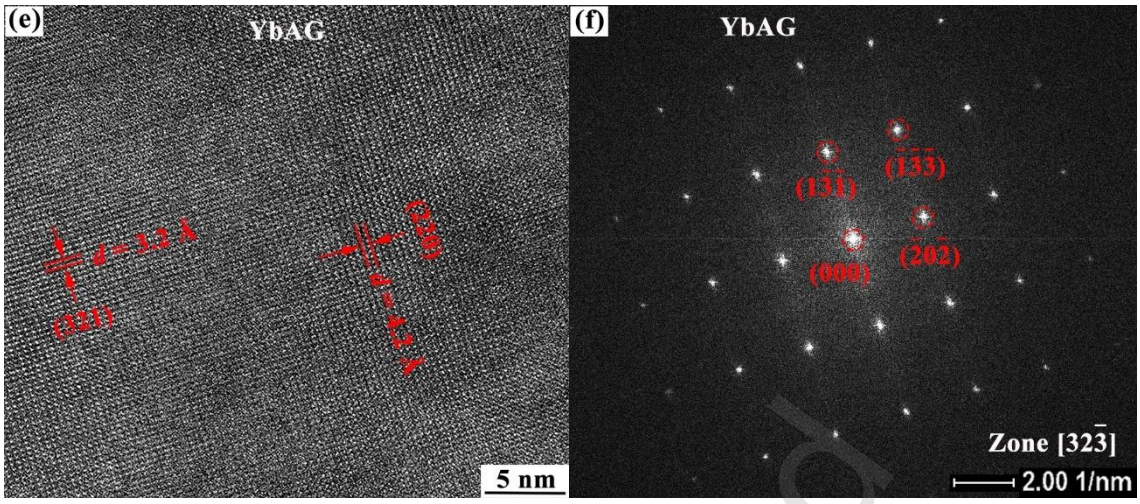

Fig. 4 Composition analysis of the surface reaction layer in the aluminum-modified coating: (a) cross-sectional image obtained in BSE mode, (b) elemental composition of the points in Fig. 3a, (c) BF image of the surface reaction layer obtained by TEM, (d) corresponding element distribution in Fig. 4c, and (e) HRTEM image and (f) SAD pattern of the block in Fig. 4c.

3.2. Structural evolution after water vapor exposure at 1350 ℃

The phase evolutions of the coatings exposed to a 50% H_2O - 50% O_2 atmosphere at 1350 ℃ for 300 h were detected, as shown in Fig. 5. The main phases of the as-sprayed and Al-modified coatings were still YbMS and YbAG, respectively. The YbAG content of the modified coating was estimated to be 66.0 wt.%, which was consistent with that before exposure, without depletion or new formation. This indicates that the YbAG phase has excellent water vapor stability and is a promising material that is resistant to water vapor and oxygen.

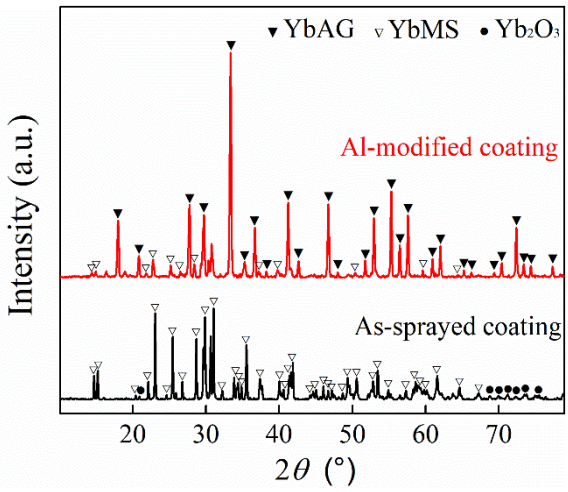

Fig. 5 XRD patterns of the as-sprayed and modified coatings after 300 h of water vapor exposure at 1350 ℃.

The microstructural evolution of the coatings after exposure to 50% H_2O-50% O_2 at 1350 ℃ for 300 h is shown in Fig. 6. Water vapor not only causes oxidation but also leads to more severe silicon volatilization corrosion. The surface of the as-sprayed EBC was in direct contact with the water vapor atmosphere, leading to significant evaporation loss of the YbMS. This exposure resulted in the formation of corrosion pits and pores and surface spallation, as shown in Figs. 6a and 6b. The internal YbMS was also significantly depleted, leaving behind porous and cracked top layers. Statistics from five cross-sectional images showed that there was approximately one channel-crack every 200 μm after exposure.

In contrast, the loss of YbMS evaporation from the aluminum-modified coating was eliminated when the coating was exposed to water vapor. The structure of the YbMS layer remained dense, without corrosion, pores, cracks, or spalling, as shown in Fig. 6c-d. The surface-formed YbAG layer was stable under high-temperature oxidative atmospheres. This created a barrier between YbMS and the corrosive atmosphere, preventing evaporation depletion by water vapor. These results confirm that a dense YbAG layer significantly improves the water vapor corrosion resistance.

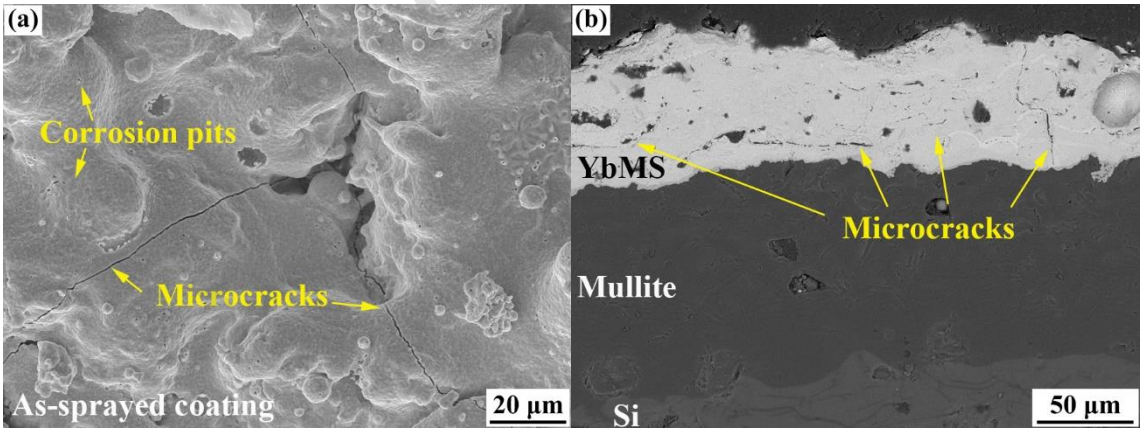

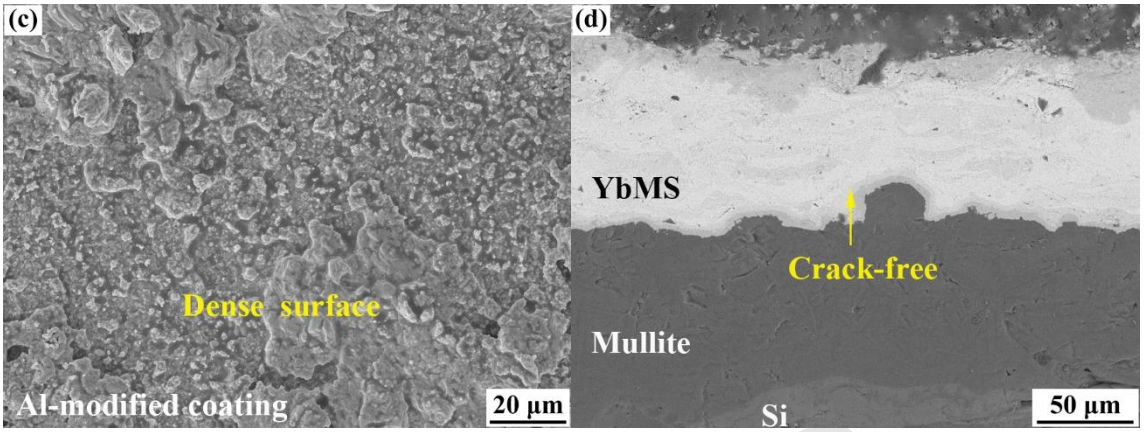

Fig. 6 Surface (a, c) and cross-sectional (b, d) microstructures of the as-sprayed and modified coatings after 300 h of water vapor exposure at 1350 ℃.

The SiO_2-TGO layer at the Si/mullite interface was further examined after exposure for 300 h, as shown in Fig. 7. The morphologies in Fig. 7a and 7b show that both the as-sprayed and modified coatings developed distinct TGO layers, whose main components were Si and O according to the line-scanning results. The porous structure of the as-sprayed coating facilitated the rapid diffusion of oxidants, such as water vapor and oxygen, leading to an accelerated oxidation rate of silicon. The measured thickness of the TGO layer reached approximately 18.5 μm. For the aluminum-modified coating, the TGO thickness decreased to approximately 4.2 μm, which was 72% thinner than that of the as-sprayed coating. A decrease in the TGO thickness is beneficial for improving the service life of EBC. These results indicate that aluminum modification can significantly increase the oxidation resistance of the as-sprayed coating.

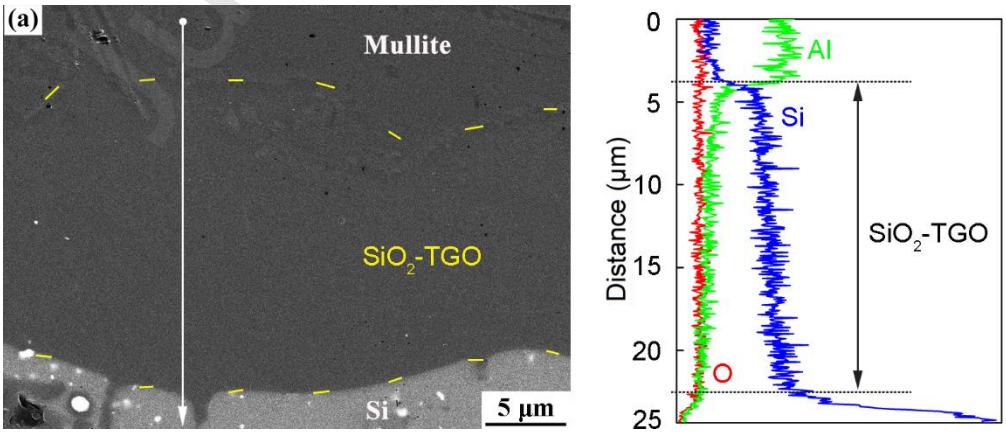

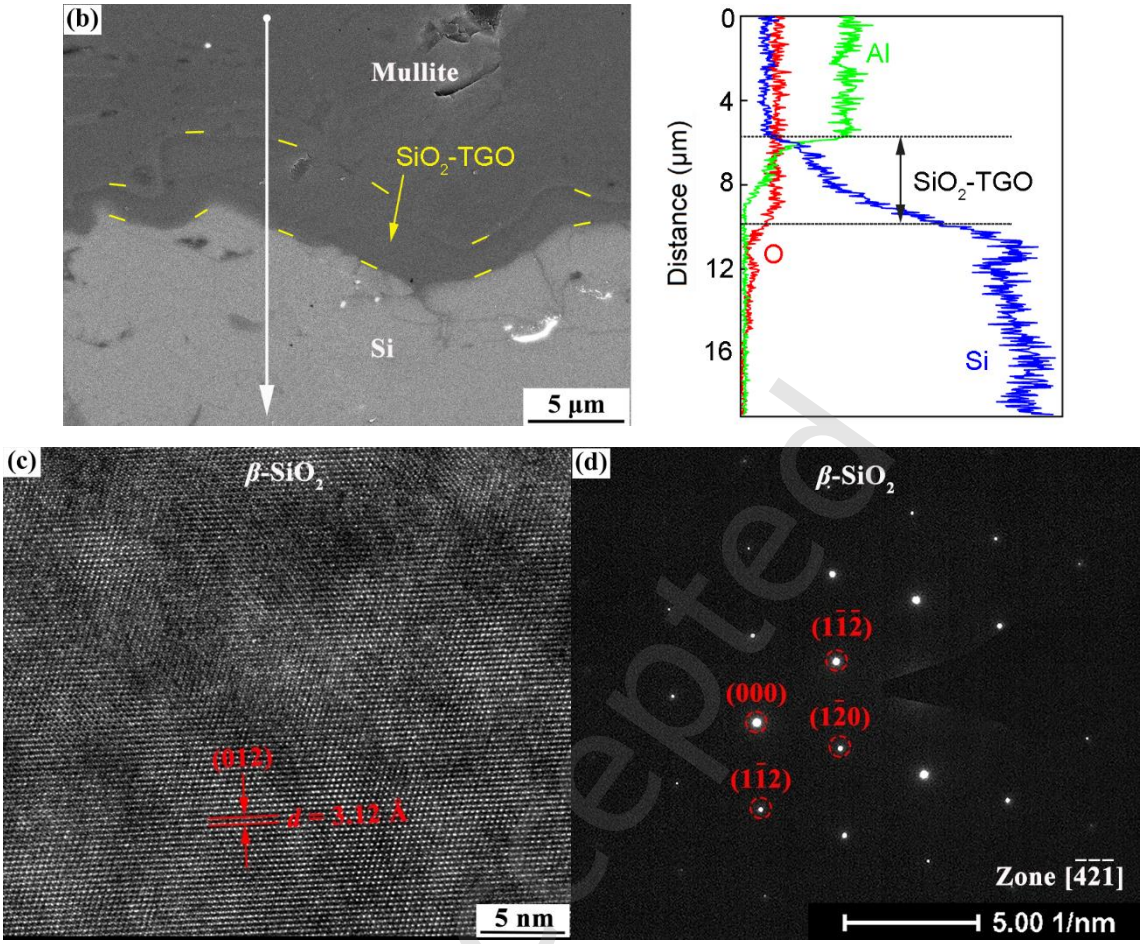

Fig. 7 Elemental distribution around the Si/mullite interface after 300 h of water vapor exposure at 1350 ℃: (a) as-sprayed coating, (b) aluminum-modified coating, (c) HRTEM image and (d) SAD pattern of SiO_2-TGO.

In addition to thickness, the structural integrity of SiO_2-TGO is also considered an important indicator of EBC life. As shown in Fig. 7, after the entire oxidation process, the TGO layers in both the porous as-sprayed coating and the dense modified coating exhibited identical structural integrity. No corrosion pores, cracks, or delamination were observed, and the layers were firmly bonded with the adjacent layers. This observation contrasts with the results reported in previous studies [21, 35]. Another phenomenon involves the detection of aluminum in the TGO layer due to the diffusion of Al from the upper mullite layer or the surface-modified layer. The contents of these two coatings were similar, approximately 20%. The structural integrity is likely attributed to the lattice modification by aluminum, which suppresses the β-α phase transformation of SiO_2, thereby inhibiting volume shrinkage and cracking [31, 33]. Additionally, the milder oxidizing environment

with lower water vapor concentrations contributed to this effect. Fig. 7c and 7d present HRTEM images of the corresponding SAD pattern of the TGO crystal structure. The interplanar spacing of the lattice fringes is approximately 0.31 nm, corresponding to the (012) plane. According to the standard PDF card (PDF 85-0621), the lattice fringe and diffraction pattern correspond to the β-SiO_2 phase, indicating that the stabilization of β-cristobalite occurred by framework alteration, which is consistent with the reported phenomenon of a Na_2O+Al_2O_3 codoped SiO_2 system [36]. However, further research is required to quantitatively analyze the inhibitory effect of these substances. These results highlighted that the modified coating formed a crack-free TGO layer during water vapor corrosion.

3.3. Isotherm oxidation kinetics of the modified coatings at 1350 ℃

The structural evolution of the TGO layer in the as-sprayed coating after various exposure times in a 50% H_2O - 50% O_2 atmosphere at 1350 ℃ is presented in Fig. 8. A distinct TGO layer of approximately 5 μm formed during the initial 50 h of exposure and subsequently thickened rapidly with increasing exposure time. The elemental distribution of Al, Si, and O near the Si/mullite interface also confirmed the growth of the TGO layer. It is worth noting that the TGO thickness exceeded 10 μm after 150 h of exposure and reached 16 μm after 300 h, which are greater than those of other groups [21, 37]. The main reason may be that the diffused aluminum changed the SiO_2 lattice and accelerated silicon oxidation.

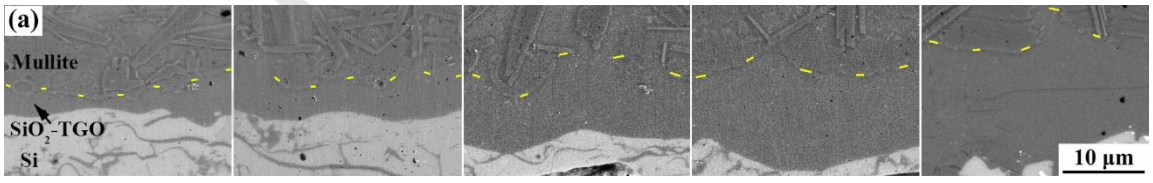

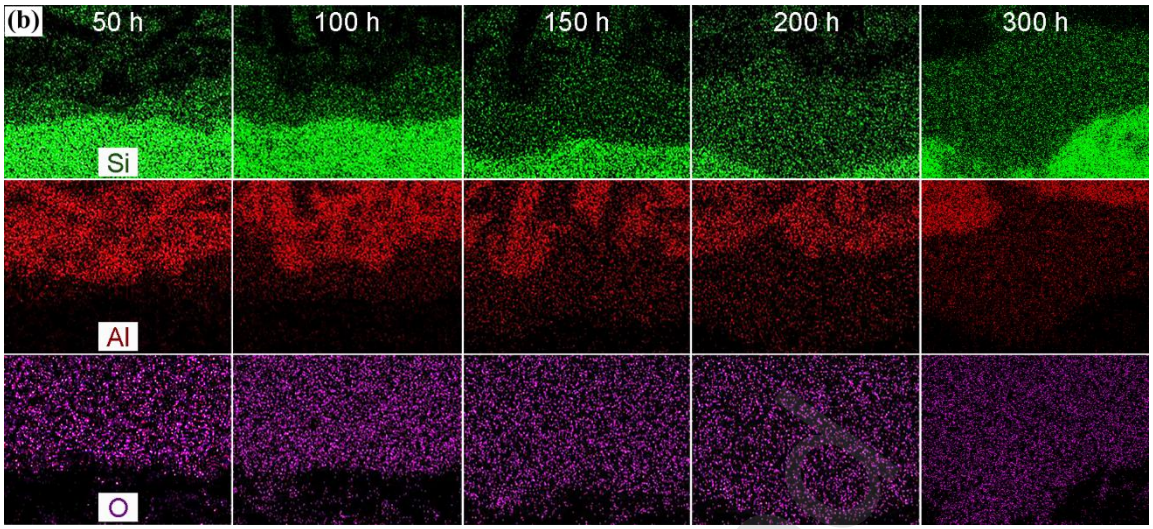

Fig. 8 Cross-sectional microstructure (a) and corresponding elemental mapping (b) of SiO_2 TGO in the as-sprayed coating after oxidation at 1350 ℃ for 50 h, 100 h, 150 h, 200 h, and 300 h.

The TGO in the aluminum-modified system exhibited a much lower growth rate than that in the as-sprayed system, as shown in Fig. 9. After 50 h of exposure, the layer was still too thin to be clearly identified. When the exposure time was extended to 100 h, the thickness of the TGO layer reached approximately 1 μm. Even after 300 h of exposure, the TGO thickness was still lower than that of the as-sprayed coating after 50 h of exposure. Several groups obtained a thicker TGO of approximately 4.0 μm in 50% H_2O-50% O_2 at a lower temperature of 1300 ℃ after 200 h of exposure [38]. This indicates that the modified coating exhibits significantly improved oxidation resistance.

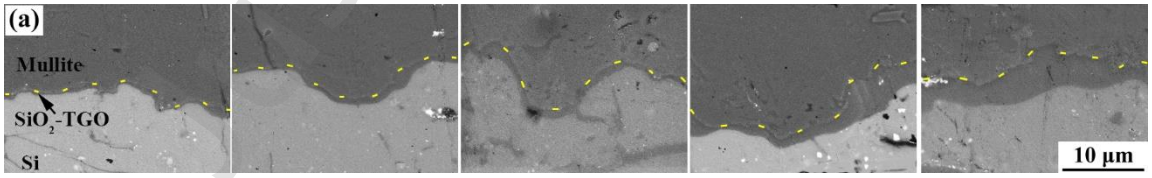

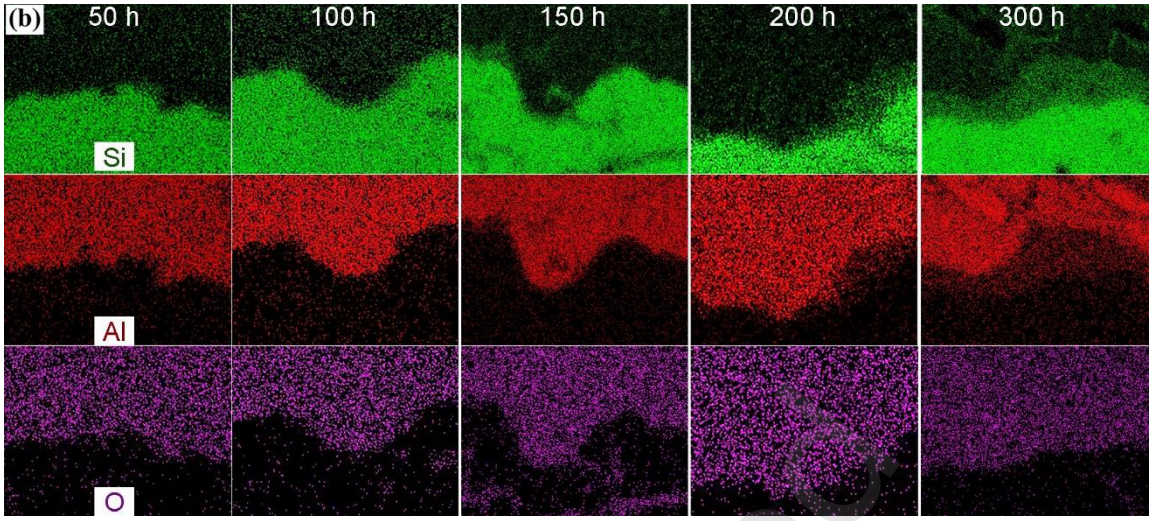

Fig. 9 Cross-sectional microstructure (a) and corresponding elemental mapping (b) of SiO_2 TGO in the modified coating after oxidation at 1350 ℃ for 50 h, 100 h, 150 h, 200 h, and 300 h.

The variation in TGO thickness with respect to exposure time and the corresponding fitted lines are shown in Fig. 10. Both exhibit approximate parabolic growth behaviors, indicating that the diffusion of oxidants dominated the oxidation rates of the Si bond coating. Obviously, the TGO thickness of the as-sprayed coatings was 4 ~ 5 times greater than that of the modified coatings during all oxidation periods. The TGO growth curves exhibited parabolic relationships, as indicated by the fitted line. The fitted parabolic rate constant, k_p, decreased from 0.86 $\mu m^2 \cdot h^{-1}$ to 0.06 $\mu m^2 \cdot h^{-1}$ after aluminum modification, nearly two orders of magnitude lower. According to the oxidation rate curves, the TGO thickness after 300 h of exposure in the modified system is equivalent to that after 25 h in the as-sprayed system, as shown by the green dotted line in Fig. 9. This indicates that aluminum modification extended the lifespan of EBC by 10 times.

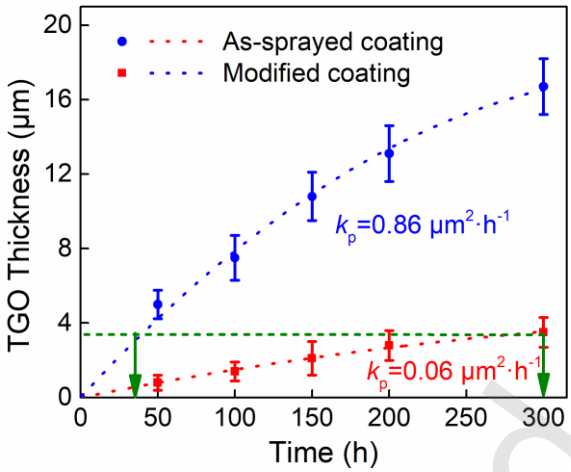

Fig. 10 Oxidation kinetics of the as-sprayed and modified coatings at 1350 °C. The dashed lines represent the line-parabolic fitting.

4. Discussion

4.1. Factors influencing the growth kinetics of the SiO_2-TGO layer

The approximately parabolic growth behavior of SiO_2-TGO demonstrated the diffusion control mechanism of oxidants, regardless of whether the EBC system was porous or dense. Water vapor and oxygen are the main oxidants in combustion environments where water vapor dominates [17-19, 38]. The transport of oxidants from the atmosphere to the Si layer must proceed through three stages, as shown in Fig. 11: (1) diffusion to the coating surface as the oxidant concentration changes from the equilibrium value c to the surface c_0; (2) diffusion through each layer, including the top layer, the mullite layer, and the SiO_2-TGO layer, to the SiO_2-TGO/Si interface, with the concentration varying from c_0 to c^*; and (3) oxidation at the silicon surface. The oxidation process is assumed to be in a steady state, so the oxidant flux is identical at each step, denoted as J. The oxygen diffusion coefficient and the thickness of the SiO_2-TGO layer are represented by D and δ, respectively.

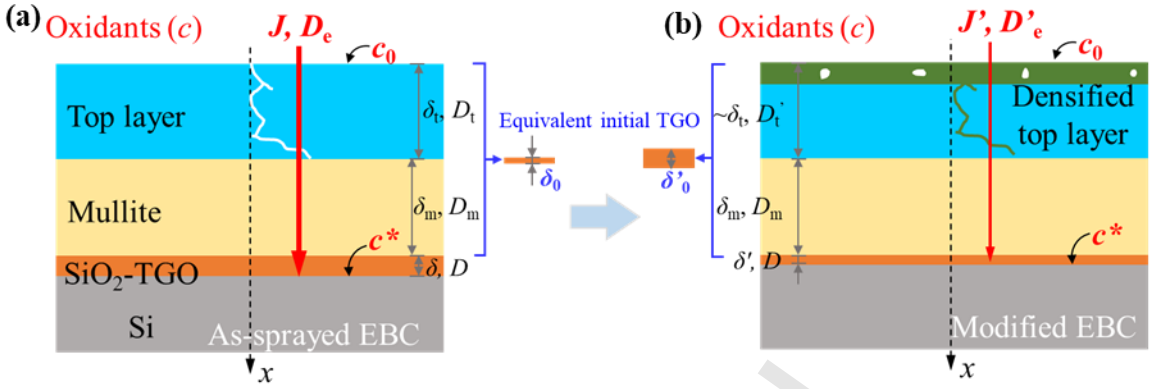

Fig. 11 Schematic diagram of oxidant diffusion from the environment to the Si bond coating in the porous as-sprayed (a) and densely modified (b) systems.

Following the well-known formulation of Deal and Grove, the oxidant flux reaching the coating surface in the first stage can be expressed as:

$$J = h\left(c_0 - c\right) \tag{1}$$

where h is the gas-phase transport coefficient.

Then, the oxidant flux from the surface to the SiO_2-TGO/Si interface in the second stage can be expressed as:

$$J = -D_e \mathrm{d}c / \mathrm{d}x \tag{2}$$

where D_e is the equivalent diffusion coefficient of the layers outside the Si bond coating.

In this work, we equate each layer to a SiO_2-TGO layer, where the equivalent thickness of the top layer is δ_t and that of the middle layer is δ_m. That is, the initial thickness of SiO_2-TGO is $\delta_0=\delta_t+\delta_m$.

According to the steady-state assumption, the equivalent initial thickness is inversely proportional to the diffusion coefficient of each layer. Thus,

$$\sum \delta_i / D_e = \sum \left(\delta_i / D_i\right) \tag{3}$$

where i represents each outside layer, including the top layer, middle layer and TGO layer, and D_i and δ_i are the diffusion coefficient and the thickness of each layer, respectively.

Thus, the equivalent initial thickness can be described as

$$\delta_0 = D\left(\delta_t / D_t + \delta_m / D_m\right) \tag{4}$$

and the equivalent diffusion coefficient:

$$D_{\mathrm{e}}=\left(\delta_{\mathrm{t}}+\delta_{\mathrm{m}}+\delta\right)/\left(\delta_{\mathrm{t}}/D_{\mathrm{t}}+\delta_{\mathrm{m}}/D_{\mathrm{m}}+\delta/D\right) \tag{5}$$

Finally, the oxidant flux corresponding to the oxidation reaction in the third stage can be expressed as:

$$J=kc^{*} \tag{6}$$

where k is the reaction rate constant.

With c_0 and c_1 eliminated, one may obtain

$$J=kc/\left(1+k/h+k\delta/D_{\mathrm{e}}\right) \tag{7}$$

The diffusion rate (dx/dt) can be described as follows:

$$\mathrm{d}x/\mathrm{d}t=J/\mathrm{N} \tag{8}$$

where N is the number of oxidant molecules incorporated per unit volume of the coating. The growth rate of SiO_2-TGO is generally believed to be controlled by the diffusion of oxygen across the SiO_2-TGO layer [31].

The oxidant transport depth x includes the SiO_2-TGO thickness δ, the assumed initial thickness and the measured SiO_2-TGO thickness during exposure. The initial condition is $x=\delta_0$ when t=0. By integrating equation (8) and obtaining the following form

$$\delta^2+\alpha\delta=k_{\mathrm{p}}\left(t+\tau\right) \tag{9}$$

where

$$\alpha=2D_e(1/k+1/h) \tag{10}$$

$$k_{\mathrm{p}}=2D_ec/\mathrm{N} \tag{11}$$

$$\tau=\left(\delta_0^2+\alpha\delta_0\right)/k_{\mathrm{p}} \tag{12}$$

Solving equation (9) can obtain

$$\delta=\alpha/2\left\{\left[1+\left(t+\tau\right)/\left(\alpha^2/4k_{\mathrm{p}}\right)\right]^{1/2}-1\right\} \tag{13}$$

Therefore, the initial thickness δ_0 causes a shift in the oxidation time but has no effect on the linear rate coefficient α or the parabolic rate coefficient k_{p}. When $t>>\alpha^2/4k_{\mathrm{p}}$ and $t>>\tau$, the equation decreases to a parabolic relationship, while when $t<<\alpha^2/4k_{\mathrm{p}}$, it can be approximated as a linear relationship. The influence on oxidation is less significant when α is small. Notably, the diffusion-controlled mechanism determines the parabolic growth

law of SiO_2-TGO, but extremely small parabolic rate constants may lead to approximately linear oxidation behavior over a long period.

4.2. Excellent oxidation mechanism of modified environmental barrier coatings

The oxygen diffusion coefficient values of each layer of the material are listed in Table 2. Water vapor significantly accelerates oxidant permeation through defect reactions in both systems [17, 39]. For the as-sprayed system, the diffusion coefficient of rare earth silicate is several orders of magnitude greater than that of SiO_2. In addition, the interconnected porous structure of the rare-earth silicate top layer and mullite middle layer (as observed in Fig. 1c and Fig. 9a) offers a fast diffusion rate of 1.98×10^{-5} $m^2 \cdot s^{-1}$, indicating that the material is nearly transparent to oxidants, whether water vapor or oxygen. In this case, the equivalent initial thickness can be ignored, i.e., δ_0=0, reducing to an approximately parabolic relationship.

Table 2 Oxygen diffusion coefficients (D) of the EBC materials

Materials	Air	YbMS	YbAG	Mullite	SiO_2
D ($m^2 \cdot s^{-1}$)	1.98×10^{-5} [40]	1.4×10^{-13} [18]	8.85×10^{-17} [41]	0.8×10^{-14}[9, 42]	3×10^{-17} [24]

Nevertheless, aluminum modification densifies the surface layer and eliminates fast diffusion channels for oxidants. Although some nanoscale pores exist, they are typically isolated and not interconnected. Moreover, a new continuous YbAG layer is formed in situ on the surface, becoming the new top layer. The intrinsic diffusion coefficient (8.85×10^{-17} $m^2 \cdot s^{-1}$) decreases to a value close to that of SiO_2 (3×10^{-17} $m^2 \cdot s^{-1}$), as listed in Table 2. Therefore, the impact of the top layer cannot be disregarded. Considering the possibility of insufficient infiltration, it was assumed that the following mullite layer would remain porous and interconnected. According to equation 12, the assumed equivalent initial thickness of SiO_2-TGO δ_0 is approximately 3~4 μm.

The phase transition of the high-temperature phase of β-SiO_2 was constrained. For current mullite-containing systems, the critical thickness (h_c) for TGO cracking can be estimated by

$$h_0 = \frac{1}{\varsigma} K_0^2 / \left[E_0 \varepsilon_0 / \left(1 - \nu_0^2\right) \right]^2 \tag{14}$$

where K_0, ν_0, ε_0, and E_0 are the fracture toughness, Poisson's ratio, dimensionless parameter, phase-transition-induced strain, and modulus, respectively. In addition, ς is a dimensionless parameter and equals 0.79. The K_{IC}, ν_0, and E_0 values are 0.77 MPa·m$^{1/2}$, -0.142, and 70 GPa, respectively. The CTEs (α) of β-SiO_2 and SiC are 3.1×10^{-6} K^{-1} and 4.67×10^{-6} K$^{-1,}$ respectively. Thus, the critical thickness for the β-SiO_2 layer is estimated to be 39 μm, which is much larger than the current value (~ 4 μm).

For the newly formed YbAG in the aluminum-modified coating, the values of α, E, ν, and K are 7.5×10^{-6} K^{-1}, 282 GPa, 0.24, and 2.77 MPa·m$^{1/2}$, respectively [1, 4-5]. The thermal mismatch stress (σ_1) was calculated to be 1143 MPa. The critical thickness (h_1) for channel cracking yields

$$h_1 = \frac{\xi}{\zeta} \frac{K_{IC}^2}{\sigma_1^2} \tag{15}$$

where the dimensionless parameter ζ represents the cracking mode and equals 1.976. The dimensionless parameter ξ is the relief factor due to the surface roughness of the actual coating and equals 0.5. Thus, the critical thickness for the YbAG layer is estimated to be 6 μm, which is consistent with the current value (5 ~ 10 μm). These results indicate that a thin YbAG layer can simultaneously improve the oxidation and cracking resistance of the EBCs.

The value of k_p is determined from the SiO_2 growth curve of the modified system in Fig. 9 and is approximately 0.06 μm^2·h^{-1}. According to equation 10, after eliminating α, the extension time is calculated to be approximately 260 h. As shown in Fig. 9, for the modified system, a TGO thickness of 3~4 μm corresponds to a lifetime of 250~300 h, while for the porous spraying system, the lifetime of the same thickness corresponds to within 50 h. This result aligns well with the predicted outcomes.

The results indicate that the structure and oxidant diffusion coefficient of the coating determine the oxidant transport resistance and lifetime in an oxidative environment. This transport resistance, denoted as R here, is analogous to the electric resistance. As shown in

Fig. 12, the transport resistance is mainly controlled by three layers, the top layer, the middle layer, and the TGO layer, which increase with increasing oxidation time. For the top layer, in addition to the lattice and grain boundary diffusion resistance (R_{top}), there is also diffusion resistance from the interconnected pores and cracks (R_{pore}). These two resistances are connected in parallel, resulting in a significant decrease in the equivalent resistance. In addition, the transportation resistance of the middle layer is represented by R_{mid}, which is considered to be identical in both systems. Supposing that the thermal growth layer is dense enough, the transport resistance is mainly provided by the SiO_2 lattice and grain boundaries, represented by R_{tgo}. The three parts are connected in series, and the length of the rectangular symbol represents the magnitude of the transport resistance.

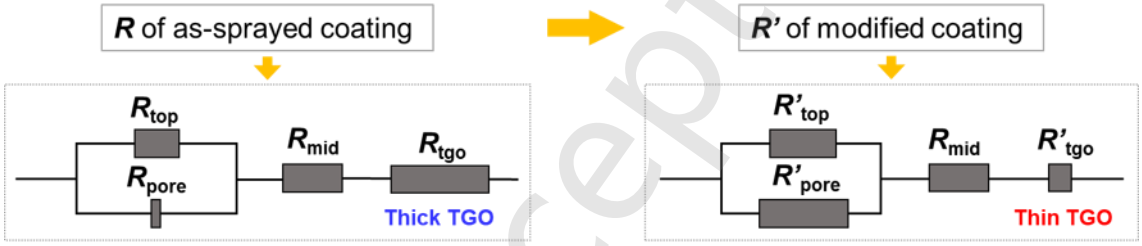

Fig. 12 Equivalent circuits used for oxidant transport in the as-sprayed (a) and modified (b) coatings. R_{top}, R'_{top}: top layer resistance; R_{pore}, R'_{pore}: pore resistance; R_{mid}, R'_{mid}: middle layer resistance; R_{tgo}, R'_{tgo}: SiO_2-TGO layer resistance.

Porous as-sprayed coatings provide interconnected pores that serve as preferential pathways for oxidant transport. The length of the resistance symbol in Fig. 11 qualitatively represents the resistance magnitude. The pore diffusion coefficient is 8~12 orders of magnitude greater than that of the coating, so the R_{pore} of the parallel part is much smaller than R_{top}. This difference determines the small transport resistance of the top layer. After densification, the fast diffusion channels are blocked, and R_{pore} increases significantly to R'_{pore}, thereby significantly improving the diffusion resistance of the parallel part. Therefore, increasing pore resistance is an effective way to inhibit oxidant transport.

In addition, replacing high oxidant diffusion coefficient materials with low coefficient materials is another helpful approach. In this work, the diffusion coefficient of YbAG formed by an in situ reaction on the surface is several orders of magnitude lower than that

of the original YbMS. which increases the transport resistance from R_{coat} to R'_{coat}. Therefore, post Al modification is verified to be a promising method for achieving a slow TGO growth rate, thereby extending the service life of the EBC system in an oxidizing environment.

5. Conclusions

An aluminum-modified YbMS/mullite/Si trilayer EBC system was prepared to enhance the oxidation resistance and extend the service life in an oxidative environment. The coatings, with and without modification, were exposed to a 50% H_2O-50% O_2 oxidative environment at 1350 °C for up to 300 hours. The following conclusions can be drawn:

(1) After aluminum modification, a dense YbAG layer formed on the coating surface, effectively eliminating interconnected pores and cracks. The porosity of the modified coating decreased to 1.1%, which is more than 80% lower than that of the as-sprayed coating.

(2) Aluminum modification significantly reduced the growth rate of SiO_2-TGO, and its thickness decreased by more than 70% after 300 h of exposure. The parabolic rate constant determined from the TGO growth curve decreased by nearly two orders of magnitude.

(3) The growth of SiO_2-TGO was controlled by the diffusion of the oxidant. Porous as-sprayed coatings are transparent to oxidants. The modified dense surface is equivalent to the initial SiO_2 layer with a specific thickness, causing a shift in the oxidation time.

(4) Due to the elimination of fast diffusion channels and the low oxygen permeability of YbAG, aluminum modification has been proven to be an effective approach for enhancing the durability of EBC in an oxidative environment.

Acknowledgments

The present project is supported by the Postdoctoral Innovative Talent Support Program (No. BX2021238) and the National Natural Science Foundation of China (No. U22A20110, No. 52301102).

Declaration of competing interest

The authors have no competing interests to declare that are relevant to the content of this article.

References

[1] Lee KN, Zhu D, Lima RS. Perspectives on environmental barrier coatings (EBCs) manufactured via air plasma spray (APS) on ceramic matrix composites (CMCs): A Tutorial Paper. *J Therm Spray Tech* 2021, **30**: 40-58.

[2] Tejero-Martin D, Bennett C, Hussain T. A review on environmental barrier coatings: History, current state of the art and future developments. *J Eur Ceram Soc* 2021, **41**: 1747-1768.

[3] Padture NP. Advanced structural ceramics in aerospace propulsion. *Nat Mater* 2016, **15**: 804-809.

[4] Hu Q, Wang Y, Guo X, et al. Oxidation resistance of SiC_f/SiC composites with three-layer environmental barrier coatings up to 1360 °C in air atmosphere. *Ceram Int* 2022, **48**: 9610-9620.

[5] Padture NP. Environmental degradation of high-temperature protective coatings for ceramic-matrix composites in gas-turbine engines. *Npj Mater Degrad* 2019, **3**: 1-6.

[6] Chen P, Xiao P, Tang X, et al. Corrosion behavior and failure mechanism of SiC whisker and c-$AlPO_4$ particle-modified novel tri-layer $Yb_2Si_2O_7$/mullite/SiC coating in burner rig tests. *J Adv Ceram* 2022, **11**(12): 1901-1917.

[7] Zhong X, Zhu T, Niu Y, et al. Effect of microstructure evolution and crystal structure on thermal properties for plasma-sprayed RE_2SiO_5 (RE = Gd, Y, Er) environmental barrier coatings. *J Mater Sci Technol* 2021, **85**: 141-151.

[8] Tian Z, Zhang J, Zhang T, et al. Toward thermal barrier coating application for rare earth silicates RE_2SiO_5 (RE= La, Nd, Sm, Eu, and Gd). *J Eur Ceram Soc* 2019, **39**: 1463-1476.

[9] Kitaoka S, Matsudaira T, Yokoe D, et al. Oxygen permeation mechanism in polycrystalline mullite at high temperatures. *J Am Ceram Soc* 2017, **100**: 3217-3226.

[10] Richards BT, Sehr S, Franqueville F de, et al. Fracture mechanisms of ytterbium monosilicate environmental barrier coatings during cyclic thermal exposure. *Acta Mater* 2016, **103**: 448-460.

[11] Lv X, Yue M, Feng X, et al. Rare earth monosilicates as oxidation resistant interphase for SiC_f/SiC CMC: Investigation of SiC_f/Yb_2SiO_5 model composites. *J Adv Ceram* 2022, **11**(5): 702-711.

[12] Wu J, Yang W, Zhang X, et al. Corrosion behavior of PS-PVD spray $Yb_2Si_2O_7$ environmental barrier coatings during continuous water vapor exposure. *Corros Sci* 2023, **210**: 110831.

[13] Deijkers JA, Wadley HNG. A duplex bond coat approach to environmental barrier coating systems. *Acta Mater* 2021, **217**: 117167.

[14] Zhang Z, Xue Z, Park Y, et al. High-temperature performance of thermal environmental barrier coatings in 90%H_2O-10%O_2 conditions at 1475 °C. *Corros Sci* 2023,

224: 111535
[15] Chen D. TGO growth behavior in environmental barrier coatings with modified silicon bond coat. *J Therm Spray Tech* 2023, 1-7.
[16] Sullivan RM. On the oxidation of the silicon bond coat in environmental barrier coatings. *J Eur Ceram Soc* 2021, **41**: 557-562.
[17] Singh S, Nganbe M, Chen K. Modeling oxygen permeability through topcoat and thermally grown oxide in dense $Yb_2Si_2O_7$ environmental barrier coatings. *J Am Ceram Soc* 2021, **104**: 6481-6495.
[18] Bakan E, Vaßen R. Oxidation kinetics of atmospheric plasma sprayed environmental barrier coatings. *J Eur Ceram Soc* 2022, **42**: 5122-5128.
[19] Wada M, Matsudaira T, Kawashima N, et al. Mass transfer in polycrystalline ytterbium disilicate under oxygen potential gradients at high temperatures. *Acta Mater* 2017, **135**: 372-381.
[20] Matsudaira T, Wada M, Kawashima N, et al. Mass transfer in polycrystalline ytterbium monosilicate under oxygen potential gradients at high temperatures. *J Eur Ceram Soc* 2021, **41**: 3150-3160.
[21] Zhao G, Xu B, Ren K, et al. Oxygen diffusion through environmental barrier coating materials. *Ceram Int* 2020, **46**: 19545-19549.
[22] McCormack S, Cao H, Martins J, et al. The effect of porosity, mixed molecular/Knudsen diffusion, and a surface barrier layer on steam corrosion of $Yb_2Si_2O_7$. *Corros Sci* 2023, **219**: 111238.
[23] Dong L, Liu MJ, Zhang XF, et al. Pressure infiltration of molten aluminum for densification of environmental barrier coatings. *J Adv Ceram* 2022, **11** (1): 145-157.
[24] Sullivan RM. Reformulation of oxide growth equations for oxidation of silicon bond coat in environmental barrier coating systems. *J Eur Ceram Soc* 2019, **39**: 5403-5409.
[25] Garcia E, Lee H, Sampath S. Phase and microstructure evolution in plasma sprayed $Yb_2Si_2O_7$ coatings. *J Eur Ceram Soc* 2019, **39**: 1477-1486.
[26] Bakan E, Marcano D, Zhou D, et al. $Yb_2Si_2O_7$ environmental barrier coatings deposited by various thermal spray techniques: A preliminary comparative study. *J Therm Spray Tech* 2017, **26**: 1011-1024.
[27] Okawa A, Nguyen ST, Wiff JP, et al. Self-healing ability, strength enhancement, and high-temperature oxidation behavior of silicon carbide-dispersed ytterbium disilicate composite for environmental barrier coatings under isothermal heat treatment. *J Eur Ceram Soc* 2022, **42**: 6170-6181.
[28] Zhang X, Wang C, Ye R, et al. Mechanism of vertical crack formation in Yb_2SiO_5 coatings deposited via plasma spray-physical vapor deposition. *J Materiomics* 2020, **6**: 102-108.
[29] Deijkers JA, Begley MR, Wadley HNG. Failure mechanisms in model thermal and environmental barrier coating systems. *J Eur Ceram Soc* 2022, **42**: 5129-5144.
[30] Richards BT, Young KA, Foucault F de, et al. Response of ytterbium disilicate-silicon environmental barrier coatings to thermal cycling in water vapor. *Acta Mater* 2016, **106**: 1-14.
[31] Lee KN. $Yb_2Si_2O_7$ Environmental barrier coatings with reduced bond coat oxidation rates via chemical modifications for long life. *J Am Ceram Soc* 2019, **102**: 1507-1521.

[32] Yilmaz E, Paksoy AH, Gibson G, et al. Constrained sintering and thermal aging behavior of electrophoretically deposited $Yb_2Si_2O_7$ environmental barrier coating. *J Eur Ceram Soc* 2023, **43**: 6427-6439.
[33] Chen L, Wang WJ, Li JH, et al. Suppressing the phase-transition-induced cracking of SiO_2 TGOs by lattice solid solution. *J Eur Ceram Soc* 2023, **43**: 3201-3215.
[34] Deijkers JA, Wadley HNG. Hafnium silicate formation during the reaction of β‐cristobalite SiO_2 and monoclinic HfO_2 particles. *J Am Ceram Soc* 2020, **103**: 5400-5410.
[35] Lee KN, Waters DL, Puleo BJ, et al. Development of oxide-based High temperature environmental barrier coatings for ceramic matrix composites via the slurry process. *J Eur Ceram Soc* 2021, **41**: 1639-1653.
[36] Chao CH, Lu HY. Stress-induced β→α-cristobalite phase transformation in (Na_2O + Al_2O_3)-codoped silica. *Mat Sci Eng A* 2002, **328**: 267–276.
[37] Arnal S, Fourcade S, Mauvy F, et al. Design of a new yttrium silicate environmental barrier coating (EBC) based on the relationship between microstructure, transport properties and protection efficiency. *J Eur Ceram Soc* 2022, **42**: 1061-1076.
[38] Lu Y, Wang Y. Formation and growth of silica layer beneath environmental barrier coatings under water-vapor environment. *J Alloy Compd* 2018, **739**: 817-826.
[39] Stack P, Kane K, Sweet M, et al. Dry air cyclic oxidation of mixed Y/Yb disilicate environmental barrier coatings and bare silica formers. *J Eur Ceram Soc* 2022, **42**: 3345-3350.
[40] Daniel H. *Introduction to environmental soil physics*: Elsevier, 2003.
[41] Kitaoka S, Matsudaira T, Kawashima N, et al. Mass transfer in $Yb_3Al_5O1_2$ films at high temperatures under oxygen potential gradients. *J Eur Ceram Soc* 2024, **44**: 1188-1201.
[42] Fielitz P, Borchardt G, Schmücker M, et al. Measurement of oxygen grain boundary diffusion in mullite ceramics by SIMS depth profiling. *Appl Surf Sci* 2003, **203**: 639-643.